

www.acsabm.org Article

# Graphene Nanocomposite Ink Coated Laser Transformed Flexible Electrodes for Selective Dopamine Detection and Immunosensing

Dipannita Ghosh, Ridma Tabassum, Pritu Parna Sarkar, MD Ashiqur Rahman, Ahmed Hasnain Jalal, Nazmul Islam,\* and Ali Ashraf\*



Cite This: ACS Appl. Bio Mater. 2024, 7, 3143-3153



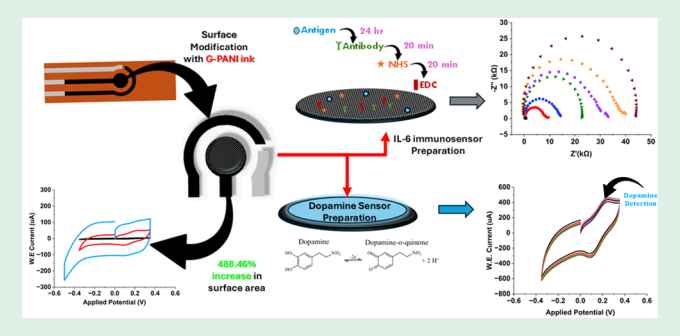
**ACCESS** I

III Metrics & More

Article Recommendations

SI Supporting Information

**ABSTRACT:** Novel and flexible disposable laser-induced graphene (LIG) sensors modified with graphene conductive inks have been developed for dopamine and interleukin-6 (IL-6) detection. The LIG sensors exhibit high reproducibility (relative standard deviation, RSD = 0.76%, N=5) and stability (RSD = 4.39%, N=15) after multiple bendings, making the sensors ideal for wearable and stretchable bioelectronics applications. We have developed electrode coatings based on graphene conductive inks, poly(3,4-ethylenedioxythiophene):polystyrene sulfonate (G-PEDOT:PSS) and polyaniline (G-PANI), for working electrode modification to improve the sensitivity and limit of detection (LOD). The



selectivity of LIG sensors modified with the G-PANI ink is 41.47 times higher than that of the screen-printed electrode with the G-PANI ink modification. We have compared our fabricated bare laser-engraved Kapton sensor (LIG) with the LIG sensors modified with G-PEDOT (LIG/G-PEDOT) and G-PANI (LIG/G-PANI) conductive inks. We have further compared the performance of the fabricated electrodes with commercially available screen-printed electrodes (SPEs) and screen-printed electrodes modified with G-PEDOT:PSS (SPE/G-PEDOT:PSS) and G-PANI (SPE/G-PANI). SPE/G-PANI has a lower LOD of 0.632  $\mu$ M compared to SPE/G-PEDOT:PSS (0.867  $\mu$ M) and SPE/G-PANI (1.974  $\mu$ M). The lowest LOD of the LIG/G-PANI sensor (0.4084  $\mu$ M, S/N = 3) suggests that it can be a great alternative to measure dopamine levels in a physiological medium. Additionally, the LIG/G-PANI electrode has excellent LOD (2.6234 pg/mL) to detect IL-6. Also, the sensor is successfully able to detect ascorbic acid (AA), dopamine (DA), and uric acid (UA) in their ternary mixture. The differential pulse voltammetry (DPV) result shows peak potential separation of 229, 294, and 523 mV for AA–DA, DA–UA, and UA–AA, respectively.

KEYWORDS: laser-induced graphene, biosensor, dopamine, IL-6, nanocomposite ink

#### 1. INTRODUCTION

As the demand for better diagnostic testing and health care monitoring increases, considerable effort has been expended in identifying biomolecules, i.e., glucose, dopamine (DA), interleukin-6 (IL-6), estrogen, cortisol, etc., that can serve as indicators of physiological responses. The implementation of analytical and electroanalytical methodologies has become increasingly crucial, as these techniques offer exceptional sensitivity and selectivity, facilitating the detection and quantitation of analytes at minimal concentrations. The nondestructive nature of specific electroanalytical methods allows for continuous assessment without compromising the sample integrity. Additionally, the capacity to concurrently determine multiple analytes from a single sample has accelerated the analytical workflow. The scientific community is continuously working toward the improvement of existing techniques and the development of new techniques for biological and environmental analysis. 1,2

Dopamine (DA) is a catecholamine neurotransmitter released throughout the central nervous system. DA

abnormalities are a symptom of neurological disorders such as Alzheimer's and Parkinson's diseases. A high dopamine level is a sign of cardiotoxicity, which can cause drug addiction, hypertension, fast heartbeats, and heart failure. Interleukin-6 (IL-6) is a pivotal pleiotropic proinflammatory cytokine. The expression of IL-6 was elevated in a concentration-dependent manner with an increase in dopamine levels. Many diseases, including osteoarthrosis, asthma, psoriasis, cardiovascular disease, diabetes, inflammatory bowel disease, COVID-19 infection, Alzheimer's disease, and prostate cancers are linked to the increasing levels of IL-6 in the blood. Because of its importance in the acute phase response to inflammation in the central nervous system, IL-6 is one of the most intensely

Received: February 4, 2024 Revised: March 24, 2024 Accepted: April 11, 2024 Published: April 25, 2024





studied biomarkers for traumatic brain injury. Due to the very low concentration of IL-6 (6 pg/mL) in healthy human serum, it is challenging to fabricate a biosensor that can be used as an earlier diagnosis of diseases.<sup>9</sup>

Improvements in sensitivity and selectivity, as well as the simplicity of the detection methodology and sensor costs, are all topics of great interest in DA and IL-6 detection. Many researchers have worked on developing new modified materials with high conductivity and large specific surface areas to improve the sensitivity of dopamine sensors including ethylenediaminetetraacetic acid (EDTA)-modified reduced graphene, 10 carbon nanofibers modified screen-printed electrode (SPE),11 palladium nanostructures on graphene oxidecellulose microfiber (GO-CMF/PdSP), 12 Au/Gr-Au composites, <sup>13</sup> poly(ethylene terephthalate) (PET)-based gold electrode, <sup>14</sup> and plasma-assisted graphene. <sup>15</sup> Mazloum-Ardakani et al. conducted a study on the electrooxidation of dopamine (DA), uric acid (UA), and their mixture using a gold electrode modified by a self-assembled monolayer of 2-(3,4-dihydroxyphenyl)-1,3-dithialone to examine the electrochemical behaviors and interactions of these compounds. 16 Several graphenebased electrodes such as graphene field-effect transistor (FET), ethanol chemical vapor deposition treatment on top of precoated GO (ECVDGO) liquid-gated field-effect transducer, 18 electrochemiluminescence (ECL), 19 (RGO)/ Fe<sub>3</sub>O<sub>4</sub>/PDDA/CdSe nanocomposites,<sup>20</sup> and carbon fibers<sup>21</sup> have been developed for the detection IL-6 biomarker. However, the complicated fabrication process of the electrodes limits practical application.

Electrochemical methods generally offer the most efficient, simple, sensitive, and selective approaches available and can easily be implemented for point-of-care (POC) testing.<sup>22</sup> Photolithography, chemical vapor deposition (CVD), and laser ablation are the most common techniques for graphene synthesis. However, these processes include expensive cleanroom techniques, high temperature or vacuum requirements, and complex chemical steps for graphene formation. Furthermore, during the postsynthesis process, graphene is transferred to a nonconductive substrate, which is both timeconsuming and expensive.<sup>23</sup> In 2014, Lin et al.<sup>24</sup> introduced a simple one-step approach for the production of threedimensional (3D) porous graphene by laser induction that has been extensively studied in the field of electroanalytical chemistry for biochemical sensing. Because of the twodimensional (2D) structural arrangement of sp<sup>2</sup>-hybridized carbon, graphene offers high thermal conductivity,<sup>25</sup> mechanical flexibility, <sup>22</sup> large surface area (~2630 m<sup>2</sup>/g), tunable band gap, self-assembly behavior, biocompatibility, and excellent conductivity.<sup>26</sup> Laser-induced graphene (LIG) is a simple process that combines the synthesis and fabrication of graphene electrodes in a single step. In this process, a laser is used to convert sp<sup>3</sup> carbon in polyimide into highly conductive hybridized sp<sup>2</sup> carbon. Under laser irradiation, the material experiences strong vibrations in the lattice structure, creating very high temperatures. These high temperatures break the C-O, C=O, and N···C bonds, drastically reducing the presence of oxygen and nitrogen within the produced laserinduced graphene. The released atoms then combine to form gases, while the material reorganizes itself to acquire the desired graphene structure.<sup>24</sup> As LIG can be easily manufactured from commercial polymers, it has been used in a variety of applications, including flexible strain gauges, 27 nonbiofouling surfaces, 28 microsupercapacitors, 29 photodetectors, 30

sound generators and detectors, 31 and electrochemical sensors.<sup>32</sup> Adding an innovative graphene conductive polymer ink on the LIG surface can increase the sensitivity and selectivity of the sensor, which has been thoroughly investigated in our study. Yang et al. have developed a laserengraved wearable sweat sensor capable of multimodal sensing for the detection of low concentrations of uric acid and tyrosine, temperature, and analytes related to diseases such as gout and metabolic disorders.<sup>33</sup> Lu et al.<sup>34</sup> worked on developing a flexible, micropatterned electrode through direct laser engraving of polyimide film enhanced with platinum nanoparticles for the construction of a hydrogen peroxide sensor and subsequently modified with glucose oxidase for sensitive glucose detection. Settu et al.<sup>35</sup> manufactured a laserinduced graphene electrode by direct UV laser engraving on polyimide tape for selective glucose detection. Tan et al. demonstrate the application of laser-scribed graphitic carbon electrodes for the detection of the inflammatory cytokine IL-6 with the limit of detection (LOD) of 5.1 pg/mL in phosphate buffer saline.30

In this study, we have developed a reliable graphene-based electrochemical biosensor and immunosensor platform that is capable of reliable, disposable, quick, and quantifiable detection of dopamine and IL-6 and is also easy to fabricate since it is a one-step method that does not require any cleanroom setup. Graphene conductive ink, poly(3,4-ethylenedioxythiophene):polystyrene sulfonate (G-PEDOT:PSS), and a novel (graphene conductive ink-polyaniline (G-PANI)) ink have been integrated with a laser-engraved sensor to fabricate the LIG/G-PEDOT:PSS and LIG/G-PANI electrodes. We first reported the LIG/G-PANI bio- and immunosensor platform and compared our novel device with a commercially available screen-printed electrode. The LOD of the LIG/G-PANI electrode for dopamine is 0.4084  $\mu$ M. The same sensor has been able to detect 2.6234 pg/mL IL-6 (95% confidence) with a 20 min response time. Also, it can simultaneously detect ascorbic acid (AA), DA, and UA, thus making it a selective dopamine sensor.

### 2. MATERIALS AND METHODS

2.1. Reagents and Apparatus. Dopamine hydrochloride, graphene nanoflakes (2-10 nm thickness, diameter approximately 5  $\mu$ m, 8000 S/m conductivity, 20–40 m<sup>2</sup>/g specific surface area, and 5 GPa tensile strength), poly(3,4-ethylenedioxythiophene)-poly-(styrenesulfonate) (PEDOT:PSS), polyaniline, phytic acid, dimethyl sulfoxide (DMSO), potassium hexacyanoferrate(III), ReagentPlus, 99% potassium hexacyanoferrate (hexacyanoferrate II) trihydrate, and silver ink was purchased from Sigma-Aldrich. Monoclonal antihuman interleukin-6 (IL-6) antibodies and IL-6 antigens were used for immune sensing and purchased from R&D Systems. The uric acid and ascorbic acid were purchased from Thermo Fisher Scientific Chemicals Inc. The commercial sensors were purchased from Metrohm Dropsens, which are  $3.4 \times 1 \times 0.05$  cm<sup>2</sup> in size. The working electrode is 4 mm in diameter. Both the working electrode and the counter electrode (CE) are made of carbon, whereas the reference electrode (RE) is made of silver. Kapton polyamide has been used as the substrate for laser-engraved sensors. A universal laser system (PLS 4.75 (60 W) 10.6  $\mu$ m CO<sub>2</sub> laser) was used to fabricate the LIG sensor, and all of the electrochemical analyses were carried out on an electrochemical workstation (Autolab Potentiostat, PGSTAT302N).

**2.2. Fabrication of Graphene Conductive Ink.** One gram of graphene nanoflakes, 0.1 g of PEDOT:PSS, 800  $\mu$ L of DMSO, and 6 mL of DI water have been used for graphene conductive PEDOT:PSS ink preparation. DMSO has been used to increase the conductivity of

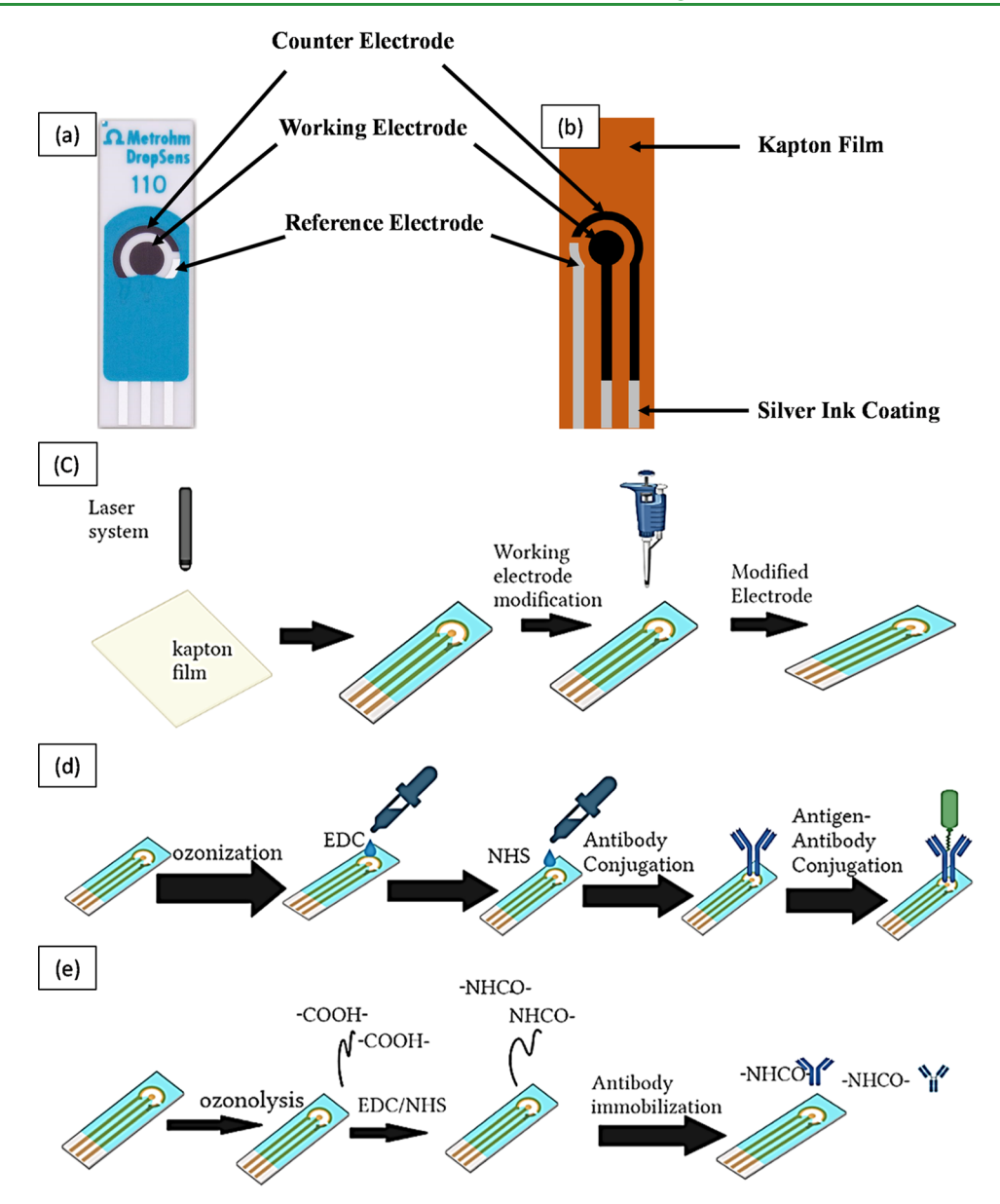


**Figure 1.** (a) Commercially available SPE sensor. (b) In-house-fabricated LIG sensor. (c) Schematic illustration of the fabrication of the electrode pattern on Kapton. (d) Schematic illustration of sensor immunization with IL-6 antigen—antibody. (e) Ethylene dichloride (EDC)—*N*-hydroxysuccinimide (NHS) chemistry for IL-6 antibody conjugation.

the ink as PEDOT:PSS has low conductivity (1 S/cm) and hydrophilicity.  $^{37}$  Graphene conductive polyaniline ink has been prepared from 1 g of graphene nanoflakes with 2 mL of polyaniline, 4 mL of phytic acid, and 6 mL of DI water.  $^{38}$  The conductivity of polyaniline increases in the acidic medium, so we used phytic acid for ink preparation. These chemicals are mixed with planetary Hauschild Speed Mixer SMART DAC 250 (mixing capacity of 250 g and speed range 300–2500 rpm) to develop a homogeneous ink solution. The experiments are conducted at room temperature (70 °F) and normal atmospheric pressure (1 atm).

**2.3. Fabrication of Electrode Patterns on Kapton.** The vector graphics software Inventor was used to design the electrode pattern. We used the Universal Laser System for engraving the electrode pattern on Kapton foil. The Kapton films (127  $\mu$ m thickness) were rinsed in alcohol for 15 min for impurity removal, washed with DI water repeatedly, and then dried naturally. We cut the Kapton foil into appropriate-sized sheets (3.4 × 1.0 × 0.05 cm³, whereas the counter electrode is 4 mm in diameter), and then borders were taped directly onto the machine's engraving table. We optimized the laser system parameter to achieve 10% power, 5–10% varied speed, 1000 pulse per

inch (PPI), and 1 mm z-axis (the height between the cutting table and laser source) for the optimal engraving and patterning of the electrode. To remove soot and other gases, the air was continuously extracted from the scribing chamber during the operation time with an exhaust flow rate of 250 cubic feet per minute (CFM). The reference electrode and the contact path were made with silver ink. After making the reference electrode and contact path with silver, the sensors were left to dry naturally for 24 h. The counter and working electrodes were made by laser transformation, and we drop cast our proposed inks only on the circular portion working electrode for modification (Figure 1a,b). The sensors were ready to use after 24 h of modification and stored in a glass container until further use. The sensor was then connected via a three-port electrode wire with Autolab Potentiostat to create a potential difference between the working and reference electrodes. We used Nova 2.1 software for data analysis.

**2.4. Fabrication of the Proposed IL-6 Immunosensors.** To prepare the sensor, a LIG/G-PANI electrode was utilized and coated with a thin poly(dimethylsiloxane) (PDMS) layer between the electrodes and contact pad to separate the working area and contact

ACS Applied Bio Materials www.acsabm.org

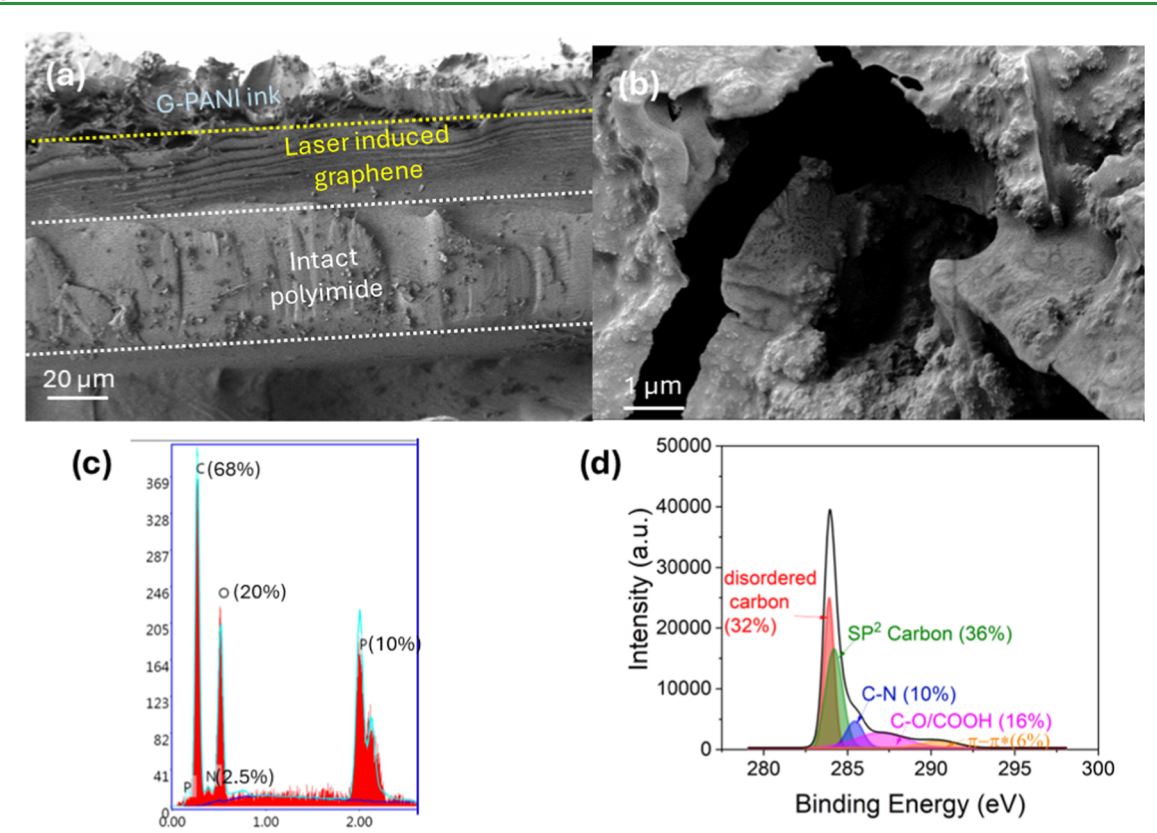


Figure 2. (a) Cross-sectional view of the sensor showing three distinct regions established by laser transformation and conformal ink coating. (b) Top view of porous G-PANI ink showing flat graphene sheets held together by PANI. (c) EDX of the sensor ink shows C, O, N, and P peaks due to the combination of graphene, polyaniline, and phytic acid (for homogeneity). (d) X-ray photoelectron spectroscopy (XPS) C 1s high-resolution spectrum of LIG electrode.

ends (Figure 1). Then, the sensor passed through ozonolysis using Novascan UV-Ozone instrument for 60 s to introduce the carboxylic group. After that, 0.4 M ethylene dichloride (EDC) was added to the working electrode, and the sensor was kept in a dark environment for 4 h. Following that, 0.4 M N-hydroxysuccinimide (NHS) was added and left in the dark environment for another 2 h. Then, 20  $\mu$ L of IL-6 antibody to cross-link with NHS was added; subsequently, the sensor was stored at 4 °C for 12 more hours. IL-6 antigen solutions with concentrations ranging from 2.5 pg/mL to 250 ng/mL were prepared using serial dilation. Two microliters of the antigen solution was added, and a sensor signal was obtained after 20 min of incubation time.

# 3. MATERIAL CHARACTERIZATION: SCANNING ELECTRON MICROSCOPY (SEM) AND X-RAY PHOTOELECTRON SPECTROSCOPY (XPS)

**3.1. SEM Characterization.** We have observed the intricate nanostructure and morphology of LIG with G-PANI ink and the ink itself by scanning electron microscopy (SEM). In the cross-section image of the G-PANI-coated LIG, we can observe three distinct areas, namely, unaffected polyimide base, laser transformed area, and G-PANI ink on top (Figure 2a). About 40% of the polyimide film after laser treatment ( $\sim$ 100  $\mu$ m) is laser-induced graphene. The presence of G-PANI ink on top creates a 3D hierarchical structure with a large surface area to interact with during biosensing (Figure 2b). Energy-dispersive X-ray (EDX) microanalysis shows strong carbon (c), oxygen (O, from mild oxidation treatment for antibody conjugation), nitrogen (N) from polyaniline, and phosphorus (P) peak from phytic acid used in ink preparation (Figure 2c).

**3.2. XPS Analysis.** X-ray photoelectron spectroscopy (XPS) stands as a robust method for characterizing the elemental states present in bulk materials. The XPS technique was employed to verify both the surface composition and the electronic valence states of the prepared G-PANI ink. By using this technique, it is possible to identify various chemical groups on the surface of the LIG substrate. XPS analysis of the samples was conducted with a Thermo Scientific K $\alpha$  XPS surface analysis instrument with a microfocused monochromated Al K $\alpha$  X-ray source at 1 eV for scans. The C 1s XPS spectra of G-PANI are shown in Figure 2d, where five distinctive carbon states were observed for the graphene-based conductive ink. The five peaks are located at 283.95 eV (disordered carbon, 32%), 284.4 eV (ordered sp<sup>2</sup>/graphitic carbon, 36%), 285.5 eV (C-N bond from polyaniline, 10%), 287.5 eV (C-O/COOH from mild oxidation for antibody conjugation, 16%), and 291.23 eV ( $\pi$ – $\pi$ \*, 6%). The two prominent peaks at 283.95 and 284.47 eV correspond to carbon atoms in ring structures; however, the latter indicates that a graphitic structure is formed (due to laser treatment) or deposited (as part of G-PANI ink).<sup>39</sup> The C in OH-C=O at 287.5 eV involves the carboxyl groups, whereas the peak at 291.23 eV represents  $\pi - \pi^*$  plasmon plasmon-excited states.<sup>40</sup> The high area percentage of the  $sp^2$  C=C bonds confirms the successful formation of graphene by laser treatment.<sup>41</sup>

#### 4. ELECTROCHEMICAL CHARACTERIZATION

**4.1. Electrochemical Characterization of G-PE-DOT:PSS and G-PANI Ink.** Electrochemical impedance spectroscopy (EIS) was used to investigate the interfacial

Article

ACS Applied Bio Materials www.acsabm.org

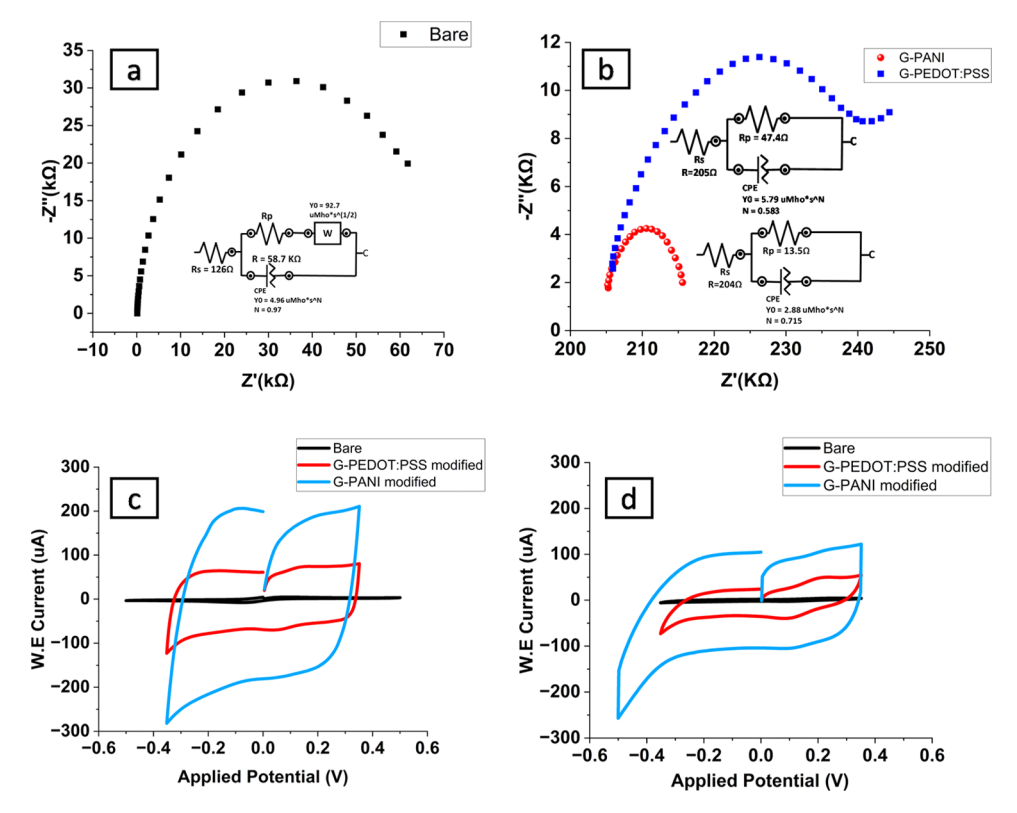


Figure 3. Electrochemical impedance data (EIS) on electrodes: (a) commercially available bare screen-printed electrode and (b) G-PEDOT:PSS ink and G-PANI ink with their equivalent Randle's circuit. Cyclic voltammograms (CV) for performance evaluation in dopamine detection (3  $\mu$ M) with 0.08 V/s scan rate of (c) SPE, SPE/G-PEDOT:PSS, and SPE/G-PANI electrodes and (d) LIG, LIG/G-PEDOT:PSS, and LIG/G-PANI electrodes.

features of the inks and compare the inks with commercial screen-printed electrodes. The usual Nyquist spectrum is composed of a low-frequency zone relating to the diffusion process and a high-frequency region corresponding to electron transfer, respectively. The Nyquist plots (frequency range 10<sup>6</sup>– 10 Hz) in Figure 3a,b are almost perfect semicircles (a characteristic of nondiffusion-limited electrochemical processes), with the diameter substantially dependent on chargetransfer resistance (R<sub>ct</sub>). The diameter of the Nyquist semicircle decreases with the increase of conductivity of the electrode surface and a shift to lower R<sub>ct</sub> values. This behavior might be explained by using a simpler (diffusion-associated impedance-free) equivalent circuit model. The smallest  $R_{ct}$ value was observed for the G-PANI ink (13.5  $\Omega$ ), compared to the G-PEDOT:PSS ink (47.4  $\Omega$ ) and a commercially available bare screen-printed electrode (58.7 k $\Omega$ ). The nonlinear line of the Nyquist plot of G-PANI ink shown in Figure 3b may be responsible for the ion transport limitation in the electrolyte within the porous electrode structure.

To evaluate the electrocatalytic activity of the proposed inks (G-PEDOT:PSS and G-PANI ink), SPE and LIG electrodes were modified with them. Figure 3c,d exhibits the cyclic voltammograms (CVs) of the proposed ink-modified screen-printed and Kapton electrodes, respectively, in the presence of 3  $\mu$ M dopamine with Fe<sup>2+</sup>/Fe<sup>3+</sup> redox couples in a basic medium (pH = 7.4). Compared to bare screen-printed electrodes (SPEs), the redox peak current increases by 16.55 and 41.47 times for the G-PEDOT:PSS ink (SPE/G-PEDOT:PSS) and G-PANI ink (SPE/G-PANI), respectively (Figure 3c). Also, for the laser-engraved Kapton sensor, the G-PANI ink (LIG/G-PANI) exhibits a higher peak current

(109.15  $\mu$ A), which is approximately 22.17 times greater than that of LIG, and the G-PEDOT:PSS(LIG/G-PEDOT:PSS) ink exhibits 20.91 times greater peak current than LIG (Figure 3d).

Article

The study demonstrates that the G-PANI and G-PEDOT:PSS ink-modified electrodes are effective for DA electrocatalytic activity detection. The greater maximum current found for the electrochemical polymerization in G-PEDOT:PSS- and G-PANI-modified electrodes is due to the electrodeposited polymer's better conductivity. The values of  $\Delta E_{\rm p}$  (the potential difference between the oxidation and reduction peak current) are 129.7, 80, and 61 mV for SPE, SPE/G-PEDOT:PSS, and SPE/G-PANI electrodes, respectively. We have further calculated the  $\Delta E_{\rm p}$  for the LIG, LIG/G-PEDOT:PSS, and LIG/G-PANI electrodes, and the values are 202, 120, and 63 mV. The smaller  $\Delta E_{\rm p}$  values represent the higher electrochemical surface area and faster electron transfer behavior. Thus, it can be said that G-PANI increased the surface area and helped to transfer electrons fast.

**4.2. Electrochemical Characterization of Fabricated Device.** The effective surface area  $(A_{\rm eff})$  of the unmodified and modified electrodes was determined from the relationship between the anodic current peak and the scan rate using the quasi-Randles–Sevcik linear equation. 42

$$I_{\rm p} = 0.436 \left( \sqrt{\frac{F^3}{RT}} \right) n^{3/2} A_{\rm eff} \sqrt{D} \, C \nu^{1/2} \tag{1}$$

Here,  $I_p$  is the anodic peak current (amperes), n is the number of mole electrons transferred during the redox reaction, F is the Faraday constant,  $A_{\text{eff}}$  is the effective surface

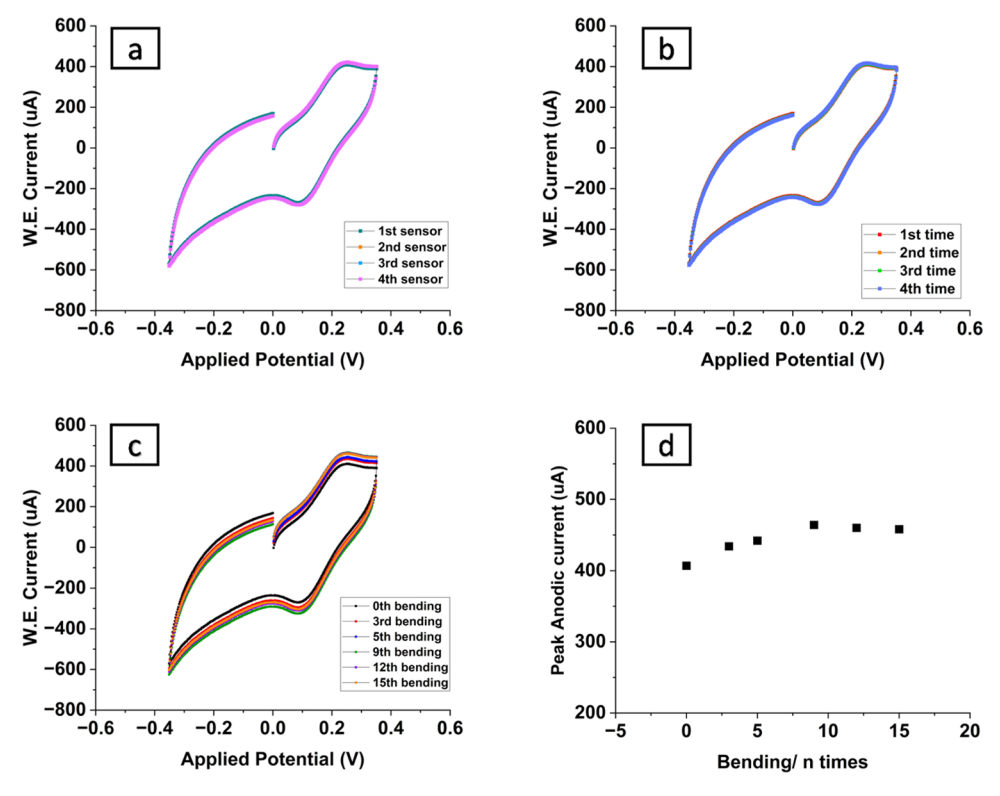


**Figure 4.** Cyclic voltammograms for 3  $\mu$ M dopamine with Fe<sup>2+</sup>/Fe<sup>3+</sup> redox couples (scan rate 0.08 V/s): (a) four distinct laser-induced sensors, (b) the same laser-induced sensor, (c) after bending the sensor multiple times, and (d) peak current vs n times bending.

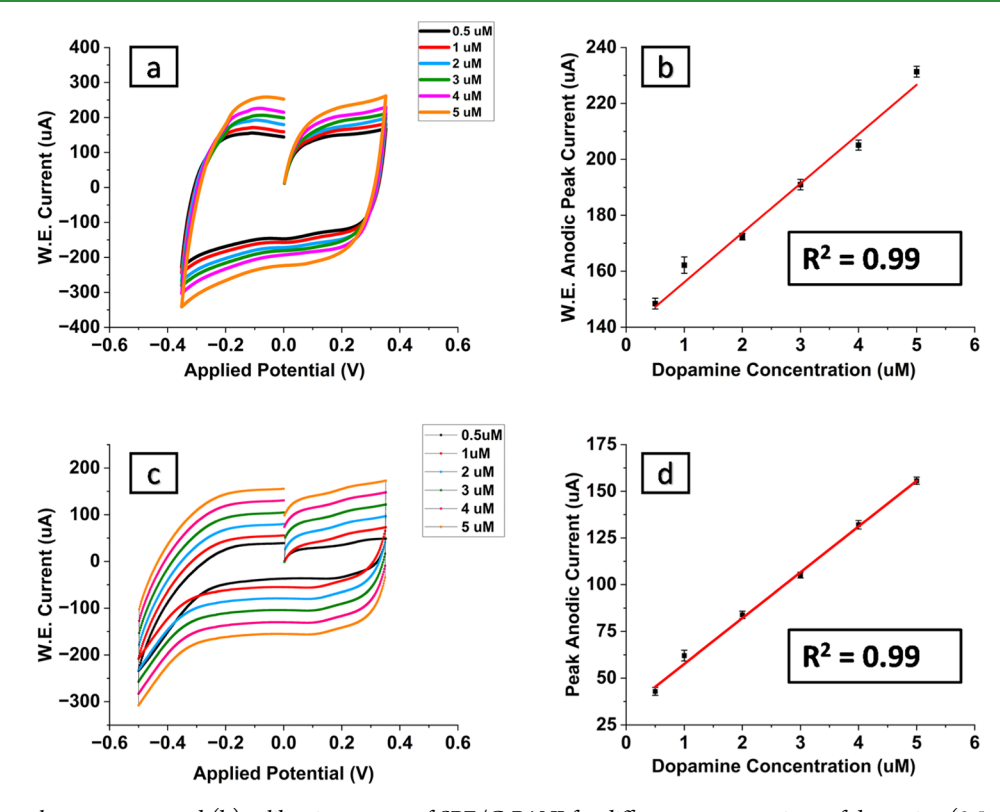


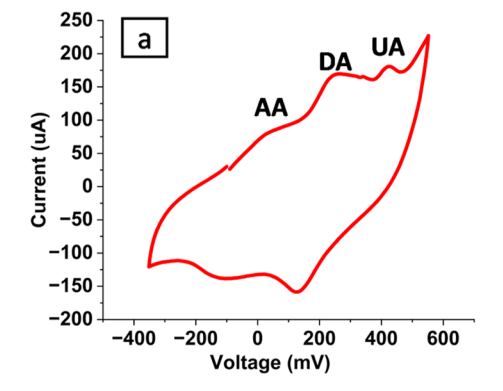
Figure 5. (a) Cyclic voltammograms and (b) calibration curves of SPE/G-PANI for different concentrations of dopamine  $(0.5-5 \,\mu\text{M})$  with a scan rate of 0.08 V/s. (c) Cyclic voltammograms and (d) calibration curves of Kapton/G-PANI for different concentrations of dopamine  $(0.5-5 \,\mu\text{M})$  with a scan rate of 0.08 V/s.

area of the electrode (cm<sup>2</sup>), C is the concentration of dopamine (mol/cm<sup>3</sup>), D is the diffusion coefficient of dopamine (7.38 × 10<sup>-6</sup> cm<sup>2</sup>/s),  $\nu$  is the scan rate (V/s), R is

the gas constant, and T is the temperature (K). We calculated the  $A_{\rm eff}$  value of the bare, G-PEDOT:PSS, and G-PANI inkmodified screen-printed electrodes to be 0.98, 1.95, and 4.73

Table 1. Comparison of LOD in Dopamine Detection between Different Electrode Materials

electrodes	detection technique	linear range $(\mu M)$	LOD $(\mu M)$	reference
SPE	CV	0.5-5	1.974	this work
SPE/G-PEDOT:PSS	CV	0.5-5	0.867	this work
SPE/G-PANI	CV	0.5-5	0.632	this work
LIG	CV	0.5-5	1.441	this work
LIG/G-PEDOT:PSS	CV	0.5-5	0.567	this work
LIG/G-PANI	CV	0.5-5	0.4084	this work
3D SWNTs-Ppy composite	amperometry	5-50	5	46
ZnO nanorod/ITO	chronoamperometry	2-777	0.45	47
GE/Au/GE/CFE	DPV	0.59-43.96	0.59	48
Ag-reduced GO/GCE	LSV	10-800	5.4	49
CTAB functionalized GO-MWCNT/GCE	DPV	5.0-500	1.5	50
Au/Gr-Aug	SW	0.3-300	0.205	13
Fe <sub>3</sub> O <sub>4</sub> @GNs/Nafion/GCE	DPV	0.020-130.0	0.007	51
$LaMnO_3$	CV	1-100	6.22	52
GME	DPV	4-100	2.64	53



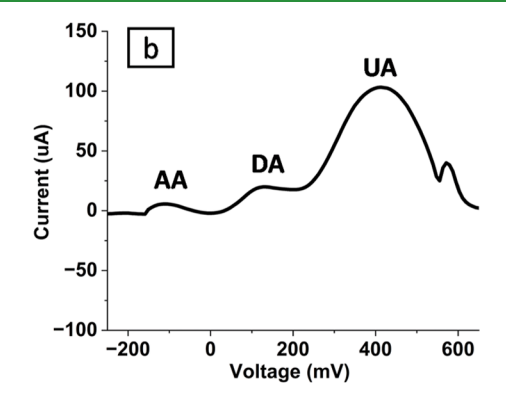


Figure 6. (a) Cyclic voltammetry (CV) and (b) differential pulse voltammetry (DPV) in a ternary mixture of 1.0 mM AA, 0.5 mM DA, and 0.8 mM UA in 1 M PBS (pH = 7.4). Scan rate of CV = 0.08 V/s. Scan rate of DPV = 0.08 V/s.

mm², respectively. The effective surface area of the working electrode modified with G-PANI ink was increased by 382.65% compared to that of the unmodified one. For the Kapton sensor, the effective surface area for the bare, G-PEDOT:PSS, and G-PANI inks is 0.78, 1.76, and 4.59 mm², respectively, which increases the effective surface area by 488.46%.

We have examined the reproducibility of the fabrication with four distinct laser-induced Kapton sensors (Figure 4a), and the analytical response was consistent with relative standard deviation (RSD) = 1.01% for  $I_p$  values (n = 4). For analytical applications, particularly point-of-need analyses, reproducible sensors are extremely important. During the experiments, the stability of the electrochemical response was also investigated by performing four cyclic voltammograms using the same electrode with a scan rate of 0.08 V/s (Figure 4b), which demonstrates excellent repeatability (RSD = 0.76% for  $I_p$ values, n = 5). The storage stability was evaluated by a laserengraved Kapton sensor after bending 15 times (Figure 4c). Our fabrication process demonstrates great stability with a value of RSD 4.39%. The anodic peak current slightly increases after bending the sensor; after 10 bendings, the peak current again decreases, and no change in peak current is observed after 12 bendings (Figure 4d). Compared to the commercial screen-printed electrodes, the laser-engraved Kapton sensors can be manufactured on a large scale without any use of chemical reagents and are also flexible.45

We have further evaluated the limit of detection (LOD) of dopamine for SPE, SPE/G-PEDOT:PSS, SPE/G-PANI, LIG,

LIG/G-PEDOT:PSS, and LIG/G-PANI electrodes using the formula

$$LOD = 3 \times \frac{S_b}{m} \tag{2}$$

over the range from 0.5 to 5  $\mu$ M. Here,  $S_b$  is the standard deviation between the blank signal, m is the slope of the calibration curve, and 3 is the signal-to-noise ratio. Our experimental range was selected to encompass both the aberrant levels often seen in Parkinson's disease and the concentrations present in bodily fluid at normal levels (1-10  $\mu$ M).<sup>44</sup> Figures 5 and S1–S4 display the current (passing between working and counter electrodes) as a function of dopamine concentration for each type of electrode. When dopamine undergoes oxidation, it is converted to dopamine quinone and gives rise to an oxidation peak in the CV method. This oxidation peak typically occurs within the range of 0.1-0.2 V at a pH of around 7.4, especially when utilizing graphene-based working electrodes. 45 The anodic peak current (IPA) has a linear relationship (coefficient of determination,  $R^2$ = 0.99) with dopamine concentrations. LIG/G-PANI sensor has the lowest LOD of 0.4084  $\mu M$  compared to other electrodes we have used in our experiment. The smaller LOD is significant when compared to other electrodes, as listed in Table 1. It can be observed that graphene-based electrodes have lower LOD compared to other electrodes. The lower LOD signifies that graphene-based electrodes can detect a lower quantity of dopamine from the absence of dopamine

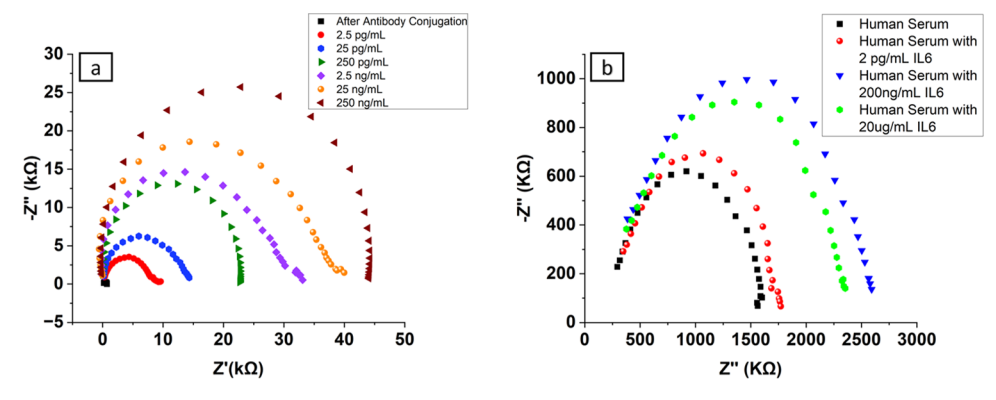


Figure 7. Electrochemical characterization (EIS) of IL-6 antibody-modified LIG/G-PANI electrodes. (a) EIS response obtained from LIG/G-PANI immunosensor with an increased IL-6 antigen concentration from 0.002 to 20 pg/mL. (b) EIS response obtained from LIG/G-PANI immunosensor in a human serum sample.

Table 2. Comparison of LOD in IL-6 Immune Sensing between Different Electrode Materials

electrodes	detection technique	linear range	LOD	references
LIG/G-PANI	EIS	0.002-20 pg/mL	2.6234 pg/mL	this work
graphene field-effect transistors		1 pM to 10 nM	8 pM	54
${ m TiO}_2$		2-2000  pg/mL	3.6 pg/mL	55
Au NPs CWNTS	SWV	0.01-800  ng/mL	2.87 pg/mL	56
SPR fiber-optic system			0.92 ng/mL	57
Au@Ag bimetallic nanoparticles			11 pg/mL with naked eye	58
bio-SPE	SWV	26-125 pg/mL	4.8 pg/mL	18
surface plasmon resonance-based essay			3.75 ng/mL	59
functionalized screen-printed electrodes	thermal	5-1000 pg/mL	3.37 pg/mL	60
4-AB/CuNSs/SPGE	DPV	0.05-500  pg/mL	0.02 pg/mL	61

with a 99% confidence level. The results indicate that the LIG/G-PANI electrode is a better choice for the detection of dopamine.

**4.3.** Selective Determination of Dopamine in the Presence of Ascorbic Acid and Uric Acid. Ascorbic acid (AA), dopamine (DA), and uric acid (UA) are all found together in various extracellular body fluids as well as human serum. These biomolecules are electrochemically active, and their oxidation potentials are quite similar to each other. Due to this, many traditional electrodes cannot distinguish their oxidation peak, and therefore, the selectivity of the sensor in testing dopamine has always been a concern.

To ensure selectivity in the sensor for dopamine detection, we used a ternary mixture of 1 mM AA, 0.5 mM DA, and 0.8 mM UA in a 1 M phosphate-buffered saline (PBS) (pH 7.4) solution containing 2.7 mM KCl. Both CV and differential pulse voltammetry (DPV) were conducted with scan rates of 50 and 80 mV/s, respectively. In the CV result (Figure 6a), the sensor showed three distinct peaks at around 27, 249, and 423 mV, which correspond to the oxidation of AA, DA, and UA, respectively. The DPV result in Figure 6b also shows three well-defined sharp peaks at -111, 118, and 412 mV for AA, DA, and UA, respectively. The calculated peak potential separations were 229 mV between AA and DA, 294 mV between DA and UA, and 523 mV between AA and UA. These calculated peak separations indicate that the detection of one biomolecule is possible in the presence of the other two, and thus, it can be concluded that the sensor is selective.

**4.4.** Electrochemical Characterization for Performance Evaluation in IL-6 Immune Sensing. In the presence of varied quantities of IL-6 antigen, the analytical performance of the engineered biosensor (LIG/G-PANI) is investigated by

using EIS techniques under optimal analysis conditions. The potentiostat performs EIS measurements, and it is responsible for exciting the biosensor between the counter electrode (CE) and the reference electrode (RE). Here, the diameter of the semicircle greatly increased after ozonolysis (shown in Figure S5b), demonstrating the modification of the sensor layer due to the large number of negative charges from carboxyl anion (-COO-) groups that inhibit the electron transfer between the modified electrode and the negatively charged redox species. The semicircle diameter increased further in the EIS after the LIG/G-PANI electrode was coated with an IL-6 antibody. The larger  $R_{ct}$  supports that the anti-IL-6 antibody has been successfully immobilized on the electrode as the hybrid IL-6 antibody film acts as a kinetic barrier for the electron transfer of the redox marker (Figure S5b). After drop casting IL-6 antigen on the working electrode area, we waited 20 min to get a stable signal (Figure S5a). An increase in  $R_{ct}$ value has been observed after binding with the IL-6 antigen, as the IL-6 antigen further inhibits the charge-transfer process (Figure S5b). Therefore, change in  $R_{ct}$  was used as an indicator for the detection of different concentrations of bioanalytes.

Figure 7a displays typical EIS curves of different IL-6 antigen concentrations within the range of 2.5 pg/mL to 250 ng/mL. A linear relationship ( $R^2=0.98$ ) was observed between the  $\Delta R_{\rm ct}$  and the IL-6 antigen concentrations with the regression equation  $\Delta R_{\rm ct}=6.2805+6.4571\times\log[{\rm IL-6}$  concentrations (pg/mL)] in Figure S5c. The LOD was 2.6234 pg/mL, which is significantly lower than the level of IL-6 in the human body (10–12 pg/mL). The results have shown that the amount of bound IL-6 antigen increased as the IL-6 concentration increased, and a protein layer was produced. This protein layer served as a nonconductive barrier and inhibited electron

transmission. In Figure 7b, IL-6 detection in human serum is shown. The results show that the sensor can detect IL-6 in human serum.

Table 2 compares the LOD performance of our studied electrodes to those of some other electrodes for IL-6 immune sensing. The LIG/G-PANI electrode has lower LOD (2.6234 pg/mL) and more sensitivity compared to other biosensors. Small amounts, i.e., 2  $\mu$ L of chemicals, are needed for the fabrication process, and the fabrication steps are also very simple. Thus, we can say that the fabricated LIG/G-PANI sensor is fast, reliable, and environmentally friendly.

#### 5. CONCLUSIONS

In this paper, a stretchable, versatile, highly sensitive, and selective laser-induced graphene bio- and immune sensors has been developed to detect dopamine and IL-6. We have further modified the working electrode of the LIG sensors with inhouse-produced graphene-based conductive inks to increase the sensitivity and selectivity of the sensors. The SEM characterization shows the surface structures of the proposed inks, and the XPS data represent the formation of major bonds on the electrode surfaces. We first reported the G-PANI ink, which is 41.47 times more sensitive for dopamine detection compared to the commercially available screen-printed sensors. We were also able to get the lowest LOD for the LIG/G-PANI sensor (0.4084  $\mu$ M) compared to the other sensors, and the selectivity of the sensor is also evident due to the formation of three different peaks (DA, UA, and AA). Our sensor also successfully detected IL-6 (LOD = 2.6234 pg/mL), and it was further tested in human serum samples for potential applications in clinical trials. Although this electrochemical immunosensor is identified to be sensitive, simple, low cost, and easy to use, it is worth noting that our fabricated sensor is not reusable, as the Ab-Ag interactions are highly stable due to their strong binding affinity. Our future goal is to develop a method to make the sensor reusable. Furthermore, we plan to automate the ink application process using a 3D printing machine to ensure a more precise addition of the ink in the working zone of the sensor. Future work will also involve the detection of other biomolecules with the sensor in real samples for diagnostics purposes.

## ASSOCIATED CONTENT

#### **Data Availability Statement**

The raw data required to reproduce these findings are available upon request from the corresponding author. The processed data required to reproduce these findings are available upon request from the corresponding author.

#### Supporting Information

The Supporting Information is available free of charge at https://pubs.acs.org/doi/10.1021/acsabm.4c00166.

Cyclic voltammograms and calibration curves for different concentrations of dopamine (0.5–5  $\mu$ M) with a scan rate of 0.08 V/s on LIG (Figure S1); cyclic voltammograms and calibration curves for different concentrations of dopamine (0.5–5  $\mu$ M) with a scan rate of 0.08 V/s on LIG/G-PEDOT-modified electrode (Figure S2); cyclic voltammograms and calibration curves for different concentrations of dopamine (0.5–5  $\mu$ M) with a scan rate of 0.08 V/s on a bare screen-printed electrode (Figure S3); cyclic voltammograms and calibration curves for different concentrations of

dopamine (0.5–5  $\mu$ M) with a scan rate of 0.08 V/s on the G-PEDOT:PSS-modified screen-printed electrode (Figure S4); and (a) incubation time to get a clear IL-6 signal, (b) immobilization process of IL-6 antibody, and (c) calibration curves of Kapton/G-PANI for different concentrations of IL-6 (Figure S5) (PDF)

#### AUTHOR INFORMATION

#### **Corresponding Authors**

Nazmul Islam – Department of Electrical and Computer Engineering, The University of Texas at Rio Grande Valley, Edinburg, Texas 78539, United States;

Email: nazmul.islam@utrgv.edu

Ali Ashraf — The University of Texas at Rio Grande Valley, Edinburg, Texas 78539, United States; orcid.org/0000-0002-7437-879X; Email: ali.ashraf@utrgv.edu

#### **Authors**

Dipannita Ghosh — Oregon State University, Corvallis, Oregon 97331, United States

Ridma Tabassum – The University of Texas at Rio Grande Valley, Edinburg, Texas 78539, United States

Pritu Parna Sarkar – The University of Texas at Rio Grande Valley, Edinburg, Texas 78539, United States

MD Ashiqur Rahman — Purdue University, West Lafayette, Indiana 47907, United States; orcid.org/0000-0001-9510-4635

Ahmed Hasnain Jalal – Department of Electrical and Computer Engineering, The University of Texas at Rio Grande Valley, Edinburg, Texas 78539, United States

Complete contact information is available at: https://pubs.acs.org/10.1021/acsabm.4c00166

#### **Author Contributions**

All authors have given approval to the final version of the manuscript.

#### Notes

The authors declare no competing financial interest.

#### ACKNOWLEDGMENTS

This research is financially supported by the National Science Foundation (NSF) under grant number ERI 2138574 and Bentsen Endowment.

#### REFERENCES

- (1) Mazloum-Ardakani, M.; Beitollahi, H.; Taleat, Z.; Naeimi, H.; Taghavinia, N. Selective Voltammetric Determination of D-Penicillamine in the Presence of Tryptophan at a Modified Carbon Paste Electrode Incorporating TiO2 Nanoparticles and Quinizarine. *J. Electroanal. Chem.* **2010**, *644* (1), 1–6.
- (2) Tajik, S.; Taher, M. A.; Beitollahi, H. First Report for Simultaneous Determination of Methyldopa and Hydrochlorothiazide Using a Nanostructured Based Electrochemical Sensor. *J. Electroanal. Chem.* **2013**, 704, 137–144.
- (3) Wang, W.; Xu, G.; Cui, X. T.; Sheng, G.; Luo, X. Enhanced Catalytic and Dopamine Sensing Properties of Electrochemically Reduced Conducting Polymer Nanocomposite Doped with Pure Graphene Oxide. *Biosens. Bioelectron.* **2014**, *58*, 153–156.
- (4) Ghosh, D.et al. In *Graphene-Conductive Polymer-Based Electro-chemical Sensor for Dopamine Detection*, Proceedings of the ASME 2022 International Mechanical Engineering Congress and Exposition. Volume 9: Mechanics of Solids, Structures, and Fluids; Micro- and Nano-Systems Engineering and Packaging; Safety Engineering, Risk, and Reliability Analysis; Research Posters. Columbus, Ohio, 2022.

- (5) Tyrrell, D. J.; Goldstein, D. R. Ageing and Atherosclerosis: Vascular Intrinsic and Extrinsic Factors and Potential Role of IL-6. *Nat. Rev. Cardiol.* **2021**, *18* (1), 58–68.
- (6) Chen, L. Y. C.; Hoiland, R. L.; Stukas, S.; Wellington, C. L.; Sekhon, M. S. Assessing the Importance of Interleukin-6 in COVID-19. *Lancet Respir. Med.* **2021**, 9 (2), No. e13.
- (7) Rothaug, M.; Becker-Pauly, C.; Rose-John, S. The Role of Interleukin-6 Signaling in Nervous Tissue. *Biochim. Biophys. Acta, Mol. Cell Res.* **2016**, *1863* (6), 1218–1227.
- (8) Zhang, K.; Liu, G.; Goldys, E. M. Robust Immunosensing System Based on Biotin-Streptavidin Coupling for Spatially Localized Femtogram mL<sup>-1</sup> Level Detection of Interleukin-6. *Biosens. Bioelectron.* **2018**, *102*, 80–86.
- (9) Kumar, L. S. S.; Wang, X.; Hagen, J.; Naik, R.; Papautsky, I.; Heikenfeld, J. Label Free Nano-Aptasensor for Interleukin-6 in Protein-Dilute Bio Fluids Such as Sweat. *Anal. Methods* **2016**, 8 (17), 3440–3444.
- (10) Hou, S.; Kasner, M. L.; Su, S.; Patel, K.; Cuellari, R. Highly Sensitive and Selective Dopamine Biosensor Fabricated with Silanized Graphene. *J. Phys. Chem. C* **2010**, *114* (35), 14915–14921.
- (11) Sharma, V.; Singh, P.; Kumar, A.; Gupta, N. Electrochemical Detection of Dopamine by Using Nickel Supported Carbon Nanofibers Modified Screen Printed Electrode. *Diamond Relat. Mater.* **2023**, 133, No. 109677.
- (12) Palanisamy, S.; Velusamy, V.; Ramaraj, S.; Chen, S.-W.; Yang, T. C. K.; Balu, S.; Banks, C. E. Facile Synthesis of Cellulose Microfibers Supported Palladium Nanospindles on Graphene Oxide for Selective Detection of Dopamine in Pharmaceutical and Biological Samples. *Mater. Sci. Eng., C* **2019**, *98*, 256–265.
- (13) Pruneanu, S.; Biris, A. R.; Pogacean, F.; Socaci, C.; Coros, M.; Rosu, M. C.; Watanabe, F.; Biris, A. S. The Influence of Uric and Ascorbic Acid on the Electrochemical Detection of Dopamine Using Graphene-Modified Electrodes. *Electrochim. Acta* **2015**, *154*, 197–204.
- (14) Wang, Y.; Wang, X.; Lu, W.; Yuan, Q.; Zheng, Y.; Yao, B. A Thin Film Polyethylene Terephthalate (PET) Electrochemical Sensor for Detection of Glucose in Sweat. *Talanta* **2019**, *198*, 86–92.
- (15) Jothi, L.; Neogi, S.; Jaganathan, S. K.; Nageswaran, G. Simultaneous Determination of Ascorbic Acid, Dopamine and Uric Acid by a Novel Electrochemical Sensor Based on N 2 /Ar RF Plasma Assisted Graphene Nanosheets/Graphene Nanoribbons. *Biosens. Bioelectron.* **2018**, *105*, 236–242.
- (16) Mazloum-Ardakani, M.; Beitollahi, H.; Amini, M. K.; Mirkhalaf, F.; Mirjalili, B.-F.; Akbari, A. Application of 2-(3, 4-Dihydroxyphen-yl)-1, 3-Dithialone Self-Assembled Monolayer on Gold Electrode as a Nanosensor for Electrocatalytic Determination of Dopamine and Uric Acid. *Analyst* **2011**, *136* (9), 1965–1970.
- (17) Hwang, M. T.; Park, I.; Heiranian, M.; Taqieddin, A.; You, S.; Faramarzi, V.; Pak, A. A.; Van Der Zande, A. M.; Aluru, N. R.; Bashir, R. Ultrasensitive Detection of Dopamine, IL-6 and SARS-CoV-2 Proteins on Crumpled Graphene FET Biosensor. *Adv. Mater. Technol.* **2021**, *6* (11), No. 2100712.
- (18) Cancelliere, R.; Di Tinno, A.; Di Lellis, A. M.; Contini, G.; Micheli, L.; Signori, E. Cost-Effective and Disposable Label-Free Voltammetric Immunosensor for Sensitive Detection of Interleukin-6. *Biosens. Bioelectron.* **2022**, 213, No. 114467.
- (19) Liu, P.-Z.; Hu, X.-W.; Mao, C.-J.; Niu, H.-L.; Song, J.-M.; Jin, B.-K.; Zhang, S.-Y. Electrochemiluminescence Immunosensor Based on Graphene Oxide Nanosheets/Polyaniline Nanowires/CdSe Quantum Dots Nanocomposites for Ultrasensitive Determination of Human Interleukin-6. *Electrochim. Acta* 2013, 113, 176–180.
- (20) Yang, Y.; Liu, Q.; Liu, X.-P.; Liu, P.-Z.; Mao, C.-J.; Niu, H.-L.; Jin, B.-K.; Zhang, S.-Y. Multifunctional Reduced Graphene Oxide (RGO)/Fe3O4/CdSe Nanocomposite for Electrochemiluminescence Immunosensor. *Electrochim. Acta* **2016**, *190*, 948–955.
- (21) Madhu, S.; Han, J. H.; Jeong, C. W.; Choi, J. Sensitive Electrochemical Sensing Platform Based on Au Nanoflower-Integrated Carbon Fiber for Detecting Interleukin-6 in Human Serum. *Anal. Chim. Acta* **2023**, *1238*, No. 340644.

- (22) Xu, Z.; Gao, C. Graphene Fiber: A New Trend in Carbon Fibers. *Mater. Today* 2015, 18 (9), 480-492.
- (23) Ye, J.; Tan, H.; Wu, S.; Ni, K.; Pan, F.; Liu, J.; Tao, Z.; Qu, Y.; Ji, H.; Simon, P.; Zhu, Y. Direct Laser Writing of Graphene Made from Chemical Vapor Deposition for Flexible, Integratable Micro-Supercapacitors with Ultrahigh Power Output. *Adv. Mater.* **2018**, *30* (27), No. 1801384.
- (24) Lin, J.; Peng, Z.; Liu, Y.; Ruiz-Zepeda, F.; Ye, R.; Samuel, E. L. G.; Yacaman, M. J.; Yakobson, B. I.; Tour, J. M. Laser-Induced Porous Graphene Films from Commercial Polymers. *Nat. Commun.* **2014**, 5 (1), No. 5714.
- (25) Balandin, A. A.; Ghosh, S.; Bao, W.; Calizo, I.; Teweldebrhan, D.; Miao, F.; Lau, C. N. Superior Thermal Conductivity of Single-Layer Graphene. *Nano Lett.* **2008**, *8* (3), 902–907.
- (26) Liu, Y.; Xu, Z.; Zhan, J.; Li, P.; Gao, C. Superb Electrically Conductive Graphene Fibers via Doping Strategy. *Adv. Mater.* **2016**, 28 (36), 7941–7947.
- (27) Rahimi, R.; Ochoa, M.; Yu, W.; Ziaie, B. Highly Stretchable and Sensitive Unidirectional Strain Sensor via Laser Carbonization. *ACS Appl. Mater. Interfaces* **2015**, *7* (8), 4463–4470.
- (28) Singh, S. P.; Li, Y.; Be'er, A.; Oren, Y.; Tour, J. M.; Arnusch, C. J. Laser-Induced Graphene Layers and Electrodes Prevents Microbial Fouling and Exerts Antimicrobial Action. ACS Appl. Mater. Interfaces 2017, 9 (21), 18238–18247.
- (29) Du, J.; Zhao, Y.; Zhang, Z.; Mu, X.; Jiang, X.; Huang, B.; Zhang, Y.; Zhang, S.; Zhang, Z.; Xie, E. High-Performance Pseudocapacitive Micro-Supercapacitors with Three-Dimensional Current Collector of Vertical ITO Nanowire Arrays. *J. Mater. Chem. A* **2019**, 7 (11), 6220–6227.
- (30) Zhang, X.; Zhang, Z.; Zhang, S.; Li, D.; Ma, W.; Ma, C.; Wu, F.; Zhao, Q.; Yan, Q.; Xing, B. Size Effect on the Cytotoxicity of Layered Black Phosphorus and Underlying Mechanisms. *Small* **2017**, *13* (32), No. 1701210.
- (31) Tao, L.-Q.; Tian, H.; Liu, Y.; Ju, Z.-Y.; Pang, Y.; Chen, Y.-Q.; Wang, D.-Y.; Tian, X.-G.; Yan, J.-C.; Deng, N.-Q.; Yang, Y.; Ren, T.-L. An Intelligent Artificial Throat with Sound-Sensing Ability Based on Laser Induced Graphene. *Nat. Commun.* **2017**, 8 (1), No. 14579.
- (32) Nayak, P.; Kurra, N.; Xia, C.; Alshareef, H. N. Highly Efficient Laser Scribed Graphene Electrodes for On-Chip Electrochemical Sensing Applications. *Adv. Electron. Mater.* **2016**, 2 (10), No. 1600185.
- (33) Yang, Y.; Song, Y.; Bo, X.; Min, J.; Pak, O. S.; Zhu, L.; Wang, M.; Tu, J.; Kogan, A.; Zhang, H.; et al. A Laser-Engraved Wearable Sensor for Sensitive Detection of Uric Acid and Tyrosine in Sweat. *Nat. Biotechnol.* **2020**, 38 (2), 217–224.
- (34) Lu, Z.; Wu, L.; Dai, X.; Wang, Y.; Sun, M.; Zhou, C.; Du, H.; Rao, H. Novel Flexible Bifunctional Amperometric Biosensor Based on Laser Engraved Porous Graphene Array Electrodes: Highly Sensitive Electrochemical Determination of Hydrogen Peroxide and Glucose. J. Hazard. Mater. 2021, 402, No. 123774.
- (35) Settu, K.; Chiu, P.-T.; Huang, Y.-M. Laser-Induced Graphene-Based Enzymatic Biosensor for Glucose Detection. *Polymers* **2021**, *13* (16), No. 2795, DOI: 10.3390/polym13162795.
- (36) Tan, P. S.; Vaughan, E.; Islam, J.; Burke, N.; Iacopino, D.; Tierney, J. B. Laser Scribing Fabrication of Graphitic Carbon Biosensors for Label-Free Detection of Interleukin-6. *Nanomaterials* **2021**, *11* (8), No. 2110, DOI: 10.3390/nano11082110.
- (37) Groenendaal, L.; Jonas, F.; Freitag, D.; Pielartzik, H.; Reynolds, J. R. Poly (3, 4-ethylenedioxythiophene) and Its Derivatives: Past, Present, and Future. *Adv. Mater.* **2000**, *12* (7), 481–494.
- (38) Ghosh, D. Graphene-Conductive Ink Coated Laser Engraved Kapton Electrochemical Biosensor for the Detection of Dopamine and Immune Sensing. The University of Texas: Rio Grande Valley, 2023
- (39) Hossain, M. F.; McCracken, S.; Slaughter, G. Electrochemical Laser Induced Graphene-Based Oxygen Sensor. *J. Electroanal. Chem.* **2021**, 899, No. 115690, DOI: 10.1016/j.jelechem.2021.115690.
- (40) Ashraf, A.; Wu, Y.; Wang, M. C.; Aluru, N. R.; Dastgheib, S. A.; Nam, S. Spectroscopic Investigation of the Wettability of Multilayer

- Graphene Using Highly Ordered Pyrolytic Graphite as a Model Material. *Langmuir* **2014**, *30* (43), 12827–12836.
- (41) Paparazzo, E. On the Interpretation of XPS Spectra of Metal (Pt, Pt-Sn) Nanoparticle/Graphene Systems. *Carbon* **2013**, *63*, 578–581.
- (42) García-Miranda Ferrari, A.; Foster, C. W.; Kelly, P. J.; Brownson, D. A.; Banks, C. E. Determination of the Electrochemical Area of Screen-Printed Electrochemical Sensing Platforms. *Biosensors* **2018**, 8 (2), No. 53, DOI: 10.3390/bios8020053.
- (43) Mendes, L. F.; de Siervo, A.; de Araujo, W. R.; Paixão, T. R. L. C. Reagentless Fabrication of a Porous Graphene-like Electrochemical Device from Phenolic Paper Using Laser-Scribing. *Carbon* **2020**, *159*, 110–118
- (44) Matt, S. M.; Gaskill, P. J. Where Is Dopamine and How Do Immune Cells See It?: Dopamine-Mediated Immune Cell Function in Health and Disease. *I. Neuroimmune Pharmacol.* **2020**, *15*, 114–164.
- (45) Balkourani, G.; Brouzgou, A.; Tsiakaras, P. A Review on Recent Advancements in Electrochemical Detection of Dopamine Using Carbonaceous Nanomaterials. *Carbon* **2023**, *213*, No. 118281.
- (46) Min, K.; Yoo, Y. J. Amperometric Detection of Dopamine Based on Tyrosinase–SWNTs–Ppy Composite Electrode. *Talanta* **2009**, *80* (2), 1007–1011.
- (47) Dong, X.-x.; Liu, Y.; Sun, Y.; Yang, C.; Xu, Z. In Situ Growth of Microporous ZnO Nanorods on ITO for Dopamine Oxidization. *Mater. Lett.* **2016**, *162*, 246–249.
- (48) Du, J.; Yue, R.; Ren, F.; Yao, Z.; Jiang, F.; Yang, P.; Du, Y. Simultaneous Determination of Uric Acid and Dopamine Using a Carbon Fiber Electrode Modified by Layer-by-Layer Assembly of Graphene and Gold Nanoparticles. *Gold Bull.* **2013**, *46*, 137–144.
- (49) Kaur, B.; Pandiyan, T.; Satpati, B.; Srivastava, R. Simultaneous and Sensitive Determination of Ascorbic Acid, Dopamine, Uric Acid, and Tryptophan with Silver Nanoparticles-Decorated Reduced Graphene Oxide Modified Electrode. *Colloids Surf., B* **2013**, *111*, 97–106
- (50) Yang, Y. J.; Li, W. CTAB Functionalized Graphene Oxide/Multiwalled Carbon Nanotube Composite Modified Electrode for the Simultaneous Determination of Ascorbic Acid, Dopamine, Uric Acid and Nitrite. *Biosens. Bioelectron.* **2014**, *56*, 300–306.
- (51) Zhang, W.; Zheng, J.; Shi, J.; Lin, Z.; Huang, Q.; Zhang, H.; Wei, C.; Chen, J.; Hu, S.; Hao, A. Nafion Covered Core—Shell Structured Fe3O4@ Graphene Nanospheres Modified Electrode for Highly Selective Detection of Dopamine. *Anal. Chim. Acta* **2015**, 853, 285–290.
- (52) Priyatharshni, S.; Divagar, M.; Viswanathan, C.; Mangalaraj, D.; Ponpandian, N. Electrochemical Simultaneous Detection of Dopamine, Ascorbic Acid and Uric Acid Using LaMnO3 Nanostructures. *J. Electrochem. Soc.* **2016**, *163* (8), B460.
- (53) Kim, Y.-R.; Bong, S.; Kang, Y.-J.; Yang, Y.; Mahajan, R. K.; Kim, J. S.; Kim, H. Electrochemical Detection of Dopamine in the Presence of Ascorbic Acid Using Graphene Modified Electrodes. *Biosens. Bioelectron.* **2010**, 25 (10), 2366–2369.
- (54) Khan, N. I.; Song, E. Detection of an IL-6 Biomarker Using a GFET Platform Developed with a Facile Organic Solvent-Free Aptamer Immobilization Approach. *Sensors* **2021**, *21* (4), No. 1335, DOI: 10.3390/s21041335.
- (55) Sakib, S.; Hosseini, A.; Zhitomirsky, I.; Soleymani, L. Photoelectrochemical IL-6 Immunoassay Manufactured on Multifunctional Catecholate-Modified TiO2 Scaffolds. ACS Appl. Mater. Interfaces 2021, 13 (43), 50851–50861.
- (56) Wang, Z.; Yang, S.; Wang, Y.; Feng, W.; Li, B.; Jiao, J.; Han, B.; Chen, Q. A Novel Oriented Immunosensor Based on AuNPs-Thionine-CMWCNTs and Staphylococcal Protein A for Interleukin-6 Analysis in Complicated Biological Samples. *Anal. Chim. Acta* 2020, 1140, 145–152.
- (57) Battaglia, T. M.; Masson, J.-F.; Sierks, M. R.; Beaudoin, S. P.; Rogers, J.; Foster, K. N.; Holloway, G. A.; Booksh, K. S. Quantification of Cytokines Involved in Wound Healing Using Surface Plasmon Resonance. *Anal. Chem.* **2005**, *77* (21), 7016–7023.

- (58) Yin, B.; Zheng, W.; Dong, M.; Yu, W.; Chen, Y.; Joo, S. W.; Jiang, X. An Enzyme-Mediated Competitive Colorimetric Sensor Based on Au@ Ag Bimetallic Nanoparticles for Highly Sensitive Detection of Disease Biomarkers. *Analyst* **2017**, *142* (16), 2954–
- (59) Deckert, F.; Legay, F. Development and Validation of an IL-6 Immuno-Receptor Assay Based on Surface Plasmon Resonance. *J. Pharm. Biomed. Anal.* **2000**, *23* (2–3), 403–411.
- (60) Crapnell, R. D.; Jesadabundit, W.; García-Miranda Ferrari, A.; Dempsey-Hibbert, N. C.; Peeters, M.; Tridente, A.; Chailapakul, O.; Banks, C. E. Toward the Rapid Diagnosis of Sepsis: Detecting Interleukin-6 in Blood Plasma Using Functionalized Screen-Printed Electrodes with a Thermal Detection Methodology. *Anal. Chem.* **2021**, 93 (14), 5931–5938.
- (61) Jesadabundit, W.; Jampasa, S.; Crapnell, R. D.; Dempsey, N. C.; Banks, C. E.; Siangproh, W.; Chailapakul, O. Toward the Rapid Diagnosis of Sepsis: Dendritic Copper Nanostructure Functionalized Diazonium Salt Modified Screen-Printed Graphene Electrode for IL-6 Detection. *Microchim. Acta* 2023, 190 (9), No. 362, DOI: 10.1007/s00604-023-05939-0.